Journal of Applied Analysis and Computation
Volume 10, Number 4, August 2020, 1355–1374
Website:http://jaac-online.com
DOI:10.11948/20190202

LIMIT CYCLE BIFURCATIONS IN THE IN-PLANE GALLOPING OF ICED TRANSMISSION LINE*

Peng Liu[1,2,3,†], Anqi Zhou[3,4], Bing Huo[5] and Xijun Liu[3,4]

Abstract In this paper, we establish a mathematical model to describe in-plane galloping of iced transmission line with geometrical and aerodynamical nonlinearities using Hamilton principle. After Galerkin Discretization, we get a two-dimensional ordinary differential equations system, further, a near Hamiltonian system is obtained by rescaling. By calculating the coefficients of the first order Melnikov function or the Abelian integral of the near-Hamiltonian system, the number of limit cycles and their locations are obtained. We demonstrate that this model can have at least 3 limit cycles in some wind velocity. Moreover, some numerical simulations are conducted to verify the theoretical results.

Keywords Galloping, limit cycle, bifurcation, Melnikov function.

MSC(2010) 37G15, 34C07.

1. Introduction

Galloping of iced transmission line is a motion involving low frequency, large amplitude and self-excited properties due to the instability of the aerodynamic forces caused by wind flow acting on the non-circular section. The classic mechanisms in galloping researches include vertical galloping mechanism by Den. Hartog [2], torsional galloping mechanism by Nigol and Buchan [17, 18], and eccentric inertia mechanism proposed by Yu et al. [22].

On the basis of above mechanism, many other galloping models were proposed. Fuhao Liu et al. established a two-degree-of-freedom model of iced, electrical quad

†the corresponding author. Email address:liupeng01@tyut.edu.cn(P. Liu)
[1]Shanxi Key Laboratory of Material Strength & Structural Impact, Taiyuan University of Technology, 79 Yingze West Street, 030024 Taiyuan, China
[2]National Demonstration Center for Experimental Mechanics Education, Taiyuan University of Technology, 79 Yingze West Street, 030024 Taiyuan, China
[3]School of Mechanical Engineering, Tianjin University, 135 Yaguan Road, 300354 Tianjin, China
[4]Tianjin Key Lab Nonlinear Dynamics and Chaos Control, Tianjin University, 135 Yaguan Road, 300354 Tianjin, China
[5]College of Mechanical Engineering, Tianjin University of Science and Technology, 1038 Dagu South Road, 300222 Tianjin, China
*The authors were supported by National Natural Science Foundation of China (51808389), Project of Shanxi Youth Foundation (201901D211067), Project of Tianjin Youth Foundation (18JCQNJC08000), and the Scientific and Technological Innovation Programs of Higher Education Institutions in Shanxi (2019L0254).

bundle conductor [10]. They analyzed co-dimension-2 bifurcation in galloping using centre manifold and invertible linear transformation. Luongo et al. proposed a new model based on curved-beam theory [13,14]. Branches of periodic solutions were obtained by employing complementary solution methods, and their stability evaluated as functions of wind velocity. Lei hou et al built a two-degree-of-freedom differential equations containing lateral and torsional motion by Lagrange equation [6]. They investigated the existence of chaotic motion in galloping system and found that there coexisted three resonance patterns in system, the mutual transformation of which may lead to chaotic motion. Zhang et al. [23] developed a useful tool for a bundle conductor of an electrical transmission line by using a three-degree-of-freedom hybrid model. This model accommodated interactions of the vertical, horizontal and torsional motions, non-linear aerodynamic loads, a non-uniform ice geometry and a variation of the wind along a span. Our team proposed a three-degree-of-freedom model to describe the nonlinear interactions between the in-plane, out-of-plane and torsional vibration [11]. Eigenvalue analysis was applied to determine the switch of different mode such as mono-modal, bi-modal and multi-modal galloping. Pierre et al. [15] explored a new approach to analyze galloping for a minimal aspect ratio of accretion shapes, by including in the quasi-static analysis the effect of the torsional vibration on the lift force. Zhaohong Qin applied Lyapunov stability theory get the critical wind speed, and obtained the effects of structural parameters to the critical wind speed [19]. Bin Liu [8] built a continuum model of the conductor galloping with D-shape ice and the aerodynamic forces were described by using the quasi steady hypothesis, where the aerodynamic coefficients were expanded by the polynomial curves with a third order and a ninth order respectively. Zhimiao Yan [21] formulated a nonlinear galloping model with regard of bending, rotation and eccentricity of cross section and the bifurcation and stability of the two cases (1:1 resonance and 2:1 resonance) were analyzed. In view of extensive literature review, we find that most of papers in galloping area focus and study equilibrium stability, internal resonance vibration, center manifold, bifurcation analysis, and even chaos, however, the limit cycle bifurcations are seldom investigated in galloping of ice transmission line. Based on our previous research, limit cycle bifurcation may be a useful tool to explore the galloping problem. Hence, the objective of the present paper is to study limit cycle bifurcations in galloping of iced transmission line. Meanwhile, our work may benefit the application of limit cycle bifurcations in engineering problem.

Limit cycle is a common phenomenon in science and engineering, and was first discovered by Poincaré. Limit cycles are generated through bifurcations in many different ways, i.e., through Hopf bifurcation from a center or a focus, via Poincaré bifurcation from closed orbits, or separatrix from homoclinic or heteroclinic orbits [4]. The most well-known 23 problems related limit cycles were presented by Hilbert [5], among which Hilbert's 16th problem is still open up to now. The second part of Hilbert's 16th problem is to find the maximal number of limit cycles and their relative locations in the planar polynomial system of degree n,

$$\dot{x} = P_n(x, y), \quad \dot{y} = Q_n(x, y),$$

where $P_n(x, y)$ and $Q_n(x, y)$ are nth-degree polynomials in x and y. Although many research results have been obtained, the precise number of limit cycles is not obtained. Then the weakened Hilbert's 16th problem was presented by Arnold [1] to help understand and attack the problem. The weakened problem is to find the

maximum number of isolated zeros of the Abelian integral or Melnikov function,

$$M(h,\delta)=\oint_{H(x,y)=h} Q_n(x,y)\mathrm{d}x - P_n(x,y)\mathrm{d}y,$$

where $H(x,y)$ is a polynomial in x and y.

A contrast on galloping models with different degree-of-freedoms was conducted by Bin Liu [9], the result showed that the one-degree-of-freedom model can also present the trend of galloping amplitude change from the point view of qualitative analysis. Hence, in this paper, we propose an one-degree-of-freedom model, which describes the in-plane motion.

The rest of paper is organized as follows. Based on Hamilton principle, the mathematical model is derived in Section 2 to describe the in-plane nonlinear vibration. Galerkin method is employed to spatially disperse the established model to get an ordinary equation system. Then using rescaling, we get a near-Hamiltonian system. The unperturbed Hamiltonian system has two centers and one saddle. Some preliminaries on limit cycle bifurcations are given in Section 3. In Section 4, we get the expansions of Melnikov functions of near-Hamiltonian system, then apply the theorem in Section 3 to obtain the number of limit cycles in present model. To verify the theoretical results, we conduct some numerical simulations in Section 5. Finally, a conclusion is drawn in Section 6.

2. Formulation of the system

The transmission line is modeled as a body made of flexible cable with length l, before modeling, we have following assumptions:

(i) The thin ice accretion is in crescent shape, and assumed to be uniform along the transmission line. The transmission line is supposed to bear tension only but not resist compression and bending moment;

(ii) The transmission tower is considered to be rigid so that the ends of the transmission line are fixed, and the sag-to-span ratio of transmission line is small, the expression of transmission line satisfies catenary equation [16];

(iii) We only consider the in-plane dynamic, which is on the basis of Den. Hartog galloping mechanism, while the axial vibration, out-of-plane vibration, and torsional vibration is ignored;

(iv) Based on the quasi-steady analysis, wind forces are evaluated at constant wind speed and angle of attack, and these wind forces are employed to galloping system.

Under above assumptions and considering the geometrical and aerodynamical nonlinearities, we establish the galloping model, the schematic of the transmission line is shown in Figure 1 (a). The transmission line is placed on the initial configuration Γ_0 under the gravity. $\bar{\Gamma}$ is the reference configuration, which swings the angle φ from Γ_0 due to the static aerodynamic forces act on the transmission line at the time $t=0$. Γ denotes the displaced configuration at the time $t>0$, and v denotes the in-plane dynamic displacements at the time t. A wind flow blows normally to the plane where Γ locates, and the aerodynamic forces produced by wind flow act on the crescent-shaped uniformly along the transmission line.

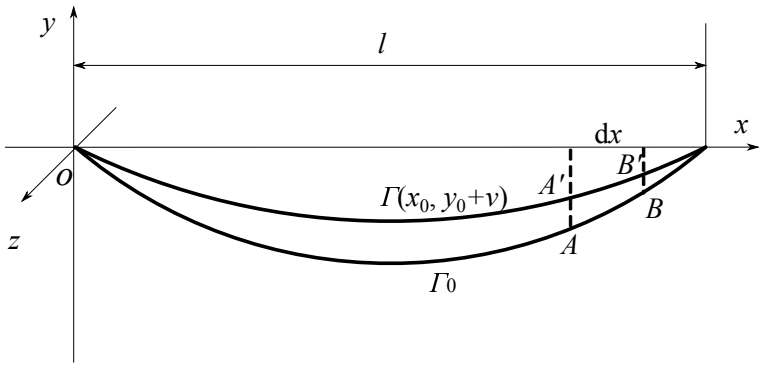

(a)

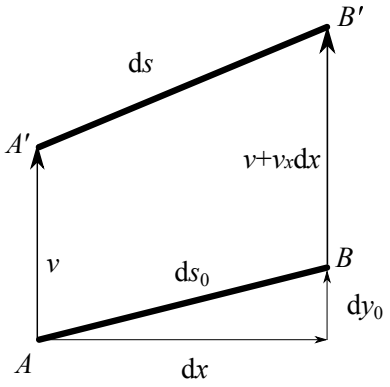

(b)

Figure 1. The theoretical model of transmission line: (a) configuration, and (b) schematic diagram of dynamic displacement.

A segment of the transmission line of an infinitesimal length dx is considered and its dynamic displacement is illustrated in Figure 1 (b), from which we have

$$\overrightarrow{AB} = \mathrm{d}x\,\vec{i} + \frac{\mathrm{d}y_0}{\mathrm{d}x}\mathrm{d}x\,\vec{j}, \tag{2.1}$$

where y_0 is the catenary equation [16] as follows

$$y_0 = -\frac{2T_0}{mg}\sinh\left(\frac{mgx}{2T_0}\right)\sinh\left[\frac{mg(l-x)}{2T_0}\right], \tag{2.2}$$

where T_0 is the initial tension of the transmission line, m is the mass per unit length of the iced transmission line, and g is gravitational acceleration constant , hereinafter, we denote $y_{0x} = \frac{\mathrm{d}y_0}{\mathrm{d}x}$.

The arc length of the segment in the reference position is obtained in the following equation

$$\mathrm{d}s_0 = \left|\overrightarrow{AB}\right| = \sqrt{1+y_{0x}^2}\mathrm{d}x \approx 1 + \frac{1}{2}y_{0x}^2 - \frac{1}{8}y_{0x}^4. \tag{2.3}$$

The vector of the deformed segment is expressed as

$$\overrightarrow{A'B'} = \mathrm{d}x\,\vec{i} + (y_{0x}+v_x)\,\mathrm{d}x\,\vec{j}, \tag{2.4}$$

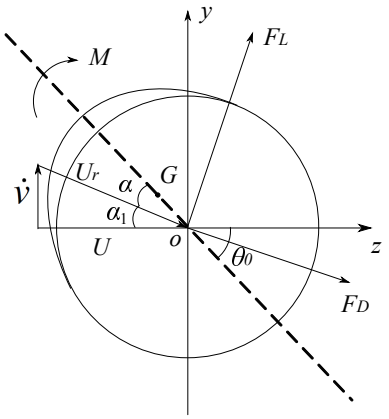

Figure 2. The schematic of velocity vector and the aerodynamics forces acting on the conductor section.

where $v_x = \frac{\mathrm{d}v}{\mathrm{d}x}$, similarly, the arc length of the deformed segment is written

$$\mathrm{d}s = \left|\overrightarrow{A'B'}\right| = \sqrt{1 + (y_{0x} + v_x)^2}\mathrm{d}x. \tag{2.5}$$

Due to the small sag-to-span ratio, we use Taylor expansion up to the third order to get the strain expression of segment, given by

$$\begin{aligned} \varepsilon &= \frac{\mathrm{d}s - \mathrm{d}s_0}{\mathrm{d}s_0} = \frac{\sqrt{1+(y_{0x}+v_x)^2}}{\sqrt{1+y_{0x}^2}} - 1 \\ &\approx (y_{0x} - y_{0x}^3)v_x + (\tfrac{1}{2} - y_{0x}^2)v_x^2 - \tfrac{1}{2}y_{0x}v_x^3. \end{aligned} \tag{2.6}$$

Then the potential energy of the transmission line is given by

$$V = \int_0^l \left(T_0 + \frac{1}{2}EA\varepsilon\right)(\mathrm{d}s - \mathrm{d}s_0) \tag{2.7}$$

where EA is the in-plane stiffness. The schematic of velocity vector and the aerodynamics forces acting on the conductor section is shown in Figure 2. Then the kinetic energy of the iced transmission line is expressed as

$$T = \int_0^l \frac{1}{2}m\dot{v}^2\mathrm{d}s_0, \tag{2.8}$$

and the virtual work performed by all forces is given

$$W = \int_0^l F_y v\mathrm{d}s_0, \tag{2.9}$$

where F_y is the aerodynamic force acting on the in-plane direction of the transmission line [22], represented as

$$F_y = F_L\cos\alpha_1 - F_D\sin\alpha_1, \tag{2.10}$$

in which F_L and F_D are lift and drag forces due to wind, α_1 is angle related to vertical velocity. The expression of F_L and F_D are:

$$\begin{aligned} F_L &= \tfrac{1}{2}\rho U_r^2 D C_L, \\ F_D &= \tfrac{1}{2}\rho U_r^2 D C_D, \end{aligned} \tag{2.11}$$

where C_L and C_D are lift and drag coefficients, ρ is the air density, D is the diameter of the bare conductor, U_r is the relative wind velocity given by $U_r = \sqrt{U^2 + \dot{v}^2}$, where U is the mean wind velocity and treated as a bifurcation parameter. Hence, F_y in (2.10) can be expressed as

$$F_y = \frac{1}{2}\rho U_r^2 D C_y, \tag{2.12}$$

in which C_y is the pure aerodynamic coefficient acting on the in-plane of the transmission. The coefficient C_y can be written as a function of the dynamical angle of attack α, i.e.,

$$C_y = r_{y_1}\alpha + r_{y_2}\alpha^2 + r_{y_3}\alpha^3, \tag{2.13}$$

where coefficients r_{y_i} $(i = 1, 2, 3)$ are obtained by curve-fitting from the experimental data in [23] and shown in Table 1, α is determined by $\alpha = \theta_0 - \alpha_1$, where θ_0 is the initial equilibrium angle of ice. For small angles, α can be expressed as $\alpha = \theta_0 - \frac{\dot{v}}{U}$.

Now, applying the Hamilton principle

$$\delta \int_{t_1}^{t_2} (T - V + W)\mathrm{d}t = 0, \tag{2.14}$$

we get the partial differential equation (PDE) of galloping of iced transmission line

$$\begin{aligned} &m\ddot{v}\left(1 + \tfrac{1}{2}y_{0x}^2 - \tfrac{1}{8}y_{0x}^4\right) + \tfrac{3}{4}EA(15y_{0x}^2 - 2)v_x^2 v_{xx} \\ &+ \left[3T_0 - \tfrac{3}{16}EAy_{0x}\left(16 - 40y_{0x}^2 - y_{0x}^4\right)\right] v_x v_{xx} \\ &+ \left[-\tfrac{1}{16}EA\left(16y_{0x}^2 + 9y_{0x}^4\right) + \tfrac{1}{2}T_0\left(3y_{0x}^2 - 2\right)\right] v_{xx} \\ &- F_y\left(1 + \tfrac{1}{2}y_{0x}^2 - \tfrac{1}{8}y_{0x}^4\right) = 0. \end{aligned} \tag{2.15}$$

where the dot denotes differentiation with respect to t.

In order to get the ordinary differential equation (ODE) of the model, we use Galerkin Discretization method

$$v(x,t) = V(t)\sin(\frac{\pi}{l}x), \tag{2.16}$$

where $V(t)$ is the dynamic displacements for the in-plane mode, and $\sin(\frac{\pi}{l}x)$ is the trail function.

Then substituting (2.16) into (2.15), and applying Galerkin procedure to get the following ODE model

$$\ddot{V} + a_1 V + 2\xi\omega\dot{V} = a_2 V^2 + a_3 V^3 + b_1\dot{V} + b_2\dot{V}^2 + b_3\dot{V}^3 + b_4\dot{V}^4 + b_5\dot{V}^5, \tag{2.17}$$

where ω and ξ is the natural frequency and the damping ratio of the in-plane vibration, respectively, a_i $(i = 1, 2, 3)$ and b_i $(i = 1, \ldots, 5)$ are the integral constants

Table 1. Conductor data and curve-fitting coefficients of C_y [23]

Parameter	Definition	Value	Units
m	Mass per unit length	2.379	kg/m
A	Cross-sectional area of iced transmission line	1017.72	mm^2
D	Diameter of bare conductor	0.0286	m
E	Elastic modulus	4.78×10^{10}	N/m^2
l	Length of the transmission line	300.0	m
ρ	Air density	1.29	kg/m^3
T	Initial tension	30000	N
θ_0	Initial equilibrium angle of ice	40	degree
ξ	Damping ratio	0.0515	
r_{y_1}	Fitting coefficient of C_y	-0.1667	
r_{y_2}	Fitting coefficient of C_y	-4.0547	
r_{y_3}	Fitting coefficient of C_y	8.3581	

related to physical parameters (see in Table 1) of transmission line, for reading convenience, the expression of $a_i\,(i = 1, 2, 3)$ and $b_i\,(i = 1, \ldots, 5)$ are given in Appendix. From the expression of $b_i\,(i = 1, \ldots, 5)$ in Appendix, we can find that b_1, b_3, b_4, b_5 are corresponding to wind velocity U, except for b_2.

Now we introduce a transformation $y = \dot{x}$ to the model (2.17) to get a second-order non-autonomous system, determined by

$$\begin{cases} \dot{x} = y, \\ \dot{y} = -a_1 x + a_2 x^2 + a_3 x^3 - 2\xi\omega y \\ \qquad +b_1 y + b_2 y^2 + b_3 y^3 + b_4 y^4 + b_5 y^5. \end{cases} \tag{2.18}$$

For convenience of analysis, we simplify the system (2.18) by the following rescalings:

$$x \to \mu_1 x, \quad y \to \mu_2 y, \quad t \to \mu_3 t, \tag{2.19}$$

where $\mu_1 = \frac{a_1}{a_2}$, $\mu_2 = \frac{a_1^{\frac{3}{2}}}{a_2}$, and $\mu_3 = \sqrt{a_1}$.

By the above, the model (2.18) is transformed to the following equivalent one:

$$\begin{cases} \dot{x} = y, \\ \dot{y} = -x + x^2 + ax^3 + b_{01}^* y + b_{02}^* y^2 + b_{03}^* y^3 + b_{04}^* y^4 + b_{05}^* y^5, \end{cases} \tag{2.20}$$

where

$$\begin{aligned} &a = \tfrac{a_3\mu_1^3}{\mu_2\mu_3}, \quad b_{01}^* = \tfrac{b_1}{\mu_3} - 2\xi, \quad b_{02}^* = \tfrac{b_2\mu_2}{\mu_3}, \\ &b_{03}^* = \tfrac{b_3\mu_2^2}{\mu_3}, \quad b_{04}^* = \tfrac{b_4\mu_2^3}{\mu_3}, \quad b_{05}^* = \tfrac{b_5\mu_2^4}{\mu_3}. \end{aligned} \tag{2.21}$$

Further, if we consider low velocity wind ($U \leq 20$m/s), then, according to (2.21) and Table 1, the coefficients $b_{0i}^*\,(i = 1, ..., 5)$ can be written as $b_{0i}^* = \varepsilon' b_{0i}\,(i = 1, ..., 5)$, $\varepsilon' \ll 1$, then the system (2.20) becomes

$$\begin{cases} \dot{x} = y, \\ \dot{y} = -x + x^2 + ax^3 + \varepsilon' \left(b_{01} y + b_{02} y^2 + b_{03} y^3 + b_{04} y^4 + b_{05} y^5\right), \end{cases} \tag{2.22}$$

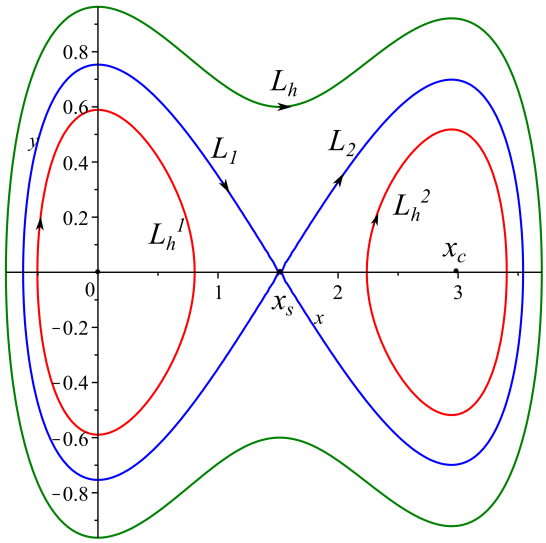

Figure 3. The phase portrait of system (2.23)

which is a near-Hamiltonian system. When $\varepsilon' = 0$, the system becomes a planar Hamiltonian system as follows

$$\begin{cases} \dot{x} = y, \\ \dot{y} = -x + x^2 + ax^3, \end{cases} \tag{2.23}$$

with the Hamiltonian function

$$H(x, y) = \frac{1}{2}y^2 + \frac{1}{2}x^2 - \frac{1}{3}x^3 - \frac{a}{4}x^4. \tag{2.24}$$

Taking parameter values from Table 1, the unperturbed system (2.23) has two elementary centers $(0, 0)$ and $(x_c, 0)$, a double homoclinic loop $L = L_1 \cup L_2$ passing through a hyperbolic saddle $(x_s, 0)$, where x_c and x_s are the roots of $-x+x^2+ax^3 = 0$, and $L_1 \equiv L|_{x<x_s}$, $L_2 \equiv L|_{x>x_s}$. The phase portrait of system (2.23) is shown in Figure 3.

Let $h_{c_1} \equiv H(0, 0) = 0$, $h_{c_2} \equiv H(x_c, 0) = 0.039412571$ and $h_s \equiv H(x_s, 0) = 0.2838521430$, we can easily get $0 \leq h_{c_1} < h_{c_2} < h_s$. In unperturbed system (2.23), there are three families of periodic orbits denoted by L_h, L_h^1 and L_h^2, respectively, where

$$\begin{aligned} L_h: &\quad H(x, y) = h, \quad h \in (h_s, +\infty); \\ L_h^1: &\quad H(x, y) = h, \quad h \in (h_{c_1}, h_s); \\ L_h^2: &\quad H(x, y) = h, \quad h \in (h_{c_2}, h_s). \end{aligned}$$

3. Preliminaries

To investigate the limit cycles bifurcation in near-Hamiltonian system (2.22), we give some preliminaries in this section. Consider a C^∞ system of form

$$\begin{aligned} \dot{x} &= H_y + \varepsilon p(x, y, \delta), \\ \dot{y} &= -H_x + \varepsilon q(x, y, \delta), \end{aligned} \tag{3.1}$$

where

$$H(x, y), \quad p(x, y, \delta) = \sum_{i+j\geq 0} a_{ij} x^i y^j, \quad q(x, y, \delta) = \sum_{i+j\geq 0} b_{ij} x^i y^j,$$

are C^∞ functions, $\varepsilon \geq 0$ is small and $\delta \in D \subset \mathbb{R}^n$ is a vector parameter with D compact. When $\varepsilon = 0$, the unperturbed system of (3.1) is

$$\begin{aligned} \dot{x} &= H_y, \\ \dot{y} &= -H_x. \end{aligned} \tag{3.2}$$

Suppose the system (3.2) has a singular point, without loss of generality, we can assume it is at origin. Then, if the singular point at the origin is elementary, we may assume

$$H(x, y) = \frac{1}{2} y^2 + h_{20} x^2 + \sum_{i+j\geq 3} h_{ij} x^i y^j, \quad h_{20} \neq 0.$$

We assume the above system has a family of periodic orbits given by $L_h = \{H(x, y) = h, \quad h \in (\alpha, \beta)\}$. The first order Melnikov function or the Abelian integral of system (3.1) is expressed as follows

$$M(h, \delta) = \oint_{L_h} q\mathrm{d}x - p\mathrm{d}y = \iint_{H\leq h} (p_x + q_y)\mathrm{d}x\mathrm{d}y, \quad h \in (\alpha, \beta), \tag{3.3}$$

the number of isolated zero roots of which relates to the number of limit cycles of sytem (3.1). For convenience, we denote $p_x + q_y = \sum_{i+j\geq 0} c_{ij} x^i y^j$.

Now we consider two different cases of singular points and give the corresponding expansion of the above Melnikov function.

- **Case 1:**
  We suppose the system (3.2) has an elementary center at the origin, and without loss of generality, we may suppose the expression of Hamiltonian function near the orgin is given by

  $$H(x, y) = \frac{\omega}{2}(x^2 + y^2) + \sum_{i+j\geq 3} h_{ij} x^i y^j, \quad \omega > 0. \tag{3.4}$$

  Then we have

Theorem 3.1 ([3]). *Let* (3.4) *hold. Then* $M(h,\delta)$ *is* C^∞ *in* $0 \le h \ll 1$ *with*

$$M(h,\delta) = h\sum_{l\ge 0} b_l(\delta)h^{l+1} + O(h^{l+1}) \tag{3.5}$$

formally for $0 \le h \ll 1$. *The expression of the coefficient* b_l *is given in [7], as follows*

$$\begin{aligned} b_0 &= 2\pi c_{00}, \\ b_1 &= c_{00}\pi\left[\tfrac{15}{2}\left(h_{30}^2+h_{03}^2\right)+\tfrac{3}{2}\left(h_{21}^2+h_{12}^2+2h_{30}h_{12}+2h_{21}h_{03}\right)\right] \\ &\quad -c_{10}\pi\left(h_{12}+3h_{30}\right)-c_{01}\pi\left(h_{21}+3h_{03}\right)+c_{20}\pi+c_{02}\pi, \\ &\cdots \end{aligned} \tag{3.6}$$

where c_{00}, c_{10}, c_{01}, c_{20} *and* c_{02} *are determined by the coefficient of* $p_x+q_y=\sum\limits_{i+j\ge 0} c_{ij}x^iy^j$.

- **Case 2:**
Suppose the system (3.2) has a double homoclinic loop $L = L_1 \cup L_2$ passing through the origin which is a hyperbolic saddle, where $L_1 = L|_{x\le 0}$ and $L_2 = L|_{x\ge 0}$. We give notation L_h to denote a family of periodic orbits defined by $H(x,y) = h$ for $0 < h \ll 1$ and $L_i(h)\,(i=1,2)$ to denote two families of periodic orbits determined by $H(x,y) = h$ for $0 < -h \ll 1$. Then, without loss of generality, we may assume

$$H(x,y) = \frac{\lambda}{2}(y^2-x^2) + \sum_{i+j\ge 3} h_{ij}x^iy^j, \quad \lambda > 0. \tag{3.7}$$

Then we have

Theorem 3.2 ([3]). *Let* (3.7) *hold. Then*

$$\begin{aligned} M(h,\delta) &= c_0(\delta) + 2c_1(\delta)h\ln|h| + c_2(\delta)h + 2c_3(\delta)h^2\ln|h| + O(h^2), \\ M_i(h,\delta) &= c_{0i}(\delta) + c_1(\delta)h\ln|h| + c_{2i}(\delta)h + c_3(\delta)h^2\ln|h| + O(h^2), \\ &\quad i=1,2, \end{aligned} \tag{3.8}$$

where

$$\begin{aligned} c_{0i}(\delta) &= \oint_{L_i} q\mathrm{d}x - p\mathrm{d}y, \quad i=1,2, \\ c_0(\delta) &= c_{01}(\delta)+c_{02}(\delta), \\ c_1(\delta) &= -\tfrac{a_{10}+b_{01}}{\lambda}, \\ c_{2i}(\delta) &= \oint_{L_i}(p_x+q_y-a_{10}-b_{01})\mathrm{d}t + b_ic_1, \quad i=1,2, \\ c_2(\delta) &= c_{21}(\delta)+c_{22}(\delta), \\ c_3(\delta) &= \ldots \end{aligned}$$

for some constants b, b_1 *and* b_2.

4. Limit cycle bifurcation analysis

4.1. Expansions of Melnikov functions of system (2.22)

In this section, we give the expansion of the related Melnikov function corresponding to system (2.22). First, we recall the results obtained in Section 2, the unperturbed system (2.23) has two elementary centers $(0,0)$ and $(x_c,0)$, a double homoclinic loop $L = L_1 \cup L_2$ passing through a hyperbolic saddle $(x_s,0)$. Hence, based on Theorem 3.1 and Theorem 3.2, the expansions of Melnikov function near $(0,0)$ and near $(x_c,0)$, the expansion of Melnikov function near the double homoclinic loop L, and the expansions of Melnikov function near L_1 and L_2 are given as follows

$$\begin{aligned} M_i(h,\delta) &= \textstyle\sum_{j=0}^{l} b_{i,j}(h-h_{ci})^j + O\left((h-h_{ci})^{j+1}\right), \\ &\quad 0 \le h - h_{ci} \ll 1, \quad i = 1,2, \end{aligned} \tag{4.1}$$

$$\begin{aligned} M(h,\delta) &= c_0(\delta) + 2c_1(\delta)(h-h_s)\ln|h-h_s| + c_2(\delta)(h-h_s) \\ &\quad +2c_3(\delta)(h-h_s)^2\ln|h-h_s| + O\left((h-h_s)^2\right), \\ &\quad 0 < h - h_s \ll 1, \end{aligned} \tag{4.2}$$

$$\begin{aligned} M_i(h,\delta) &= c_{0i}(\delta) + c_1(\delta)(h-h_s)\ln|h-h_s| + c_{2i}(\delta)(h-h_s) \\ &\quad +c_3(h-h_s)^2\ln|h-h_s| + O\left((h-h_s)^2\right), \\ &\quad 0 < h_s - h \ll 1, \quad i = 1,2. \end{aligned} \tag{4.3}$$

Now we give the coefficients of the expansion of $M_i(h,\delta)$, $i = 1,2$, and $M(h,\delta)$. To obtain the coefficients $b_{1,j}(\delta)$ in (4.1), firstly, we give the expression of the Hamiltonian function of system $(2.22)|_{\varepsilon'=0}$ as follows,

$$H(x,y) = \frac{1}{2}y^2 + \frac{1}{2}x^2 + h_{30}x^3 + h_{40}x^4,$$

where $h_{30} = -\frac{1}{3}$ and $h_{40} = -\frac{a}{4}$.

Then, using formula in Theorem 3.1, we get

$$b_{1,0} = 2\pi b_{01}, \quad b_{1,1} = \frac{15}{2}\pi b_{01}h_{30}^2 + b_{03}\pi, \quad \dots$$

Here we need to note that we only give the formulas of $b_{1,0}$ and $b_{1,1}$, since we have mentioned in section 2 that we only have one bifurcation parameter U in this system.

To obtain the coefficients $b_{2,j}(\delta)$ in (4.1), we introduce a transformation

$$u = \sqrt{\hat{\mu}}(x - x_c), \quad v = y,$$

and a time scaling $t \to \sqrt{\hat{\mu}}t$, where $\hat{\mu} = 1 - 2x_c - 3ax_c^2 > 0$.

Then the system (2.22) becomes

$$\begin{cases} \dot{u} = v, \\ \dot{v} = -u + \frac{1}{\hat{\mu}^{\frac{3}{2}}}(1+3ax_c)u^2 + \frac{a}{\hat{\mu}^2}u^3 \\ \qquad +\frac{1}{\sqrt{\hat{\mu}}}\varepsilon\left(b_{01}v + b_{02}v^2 + b_{03}v^3 + b_{04}v^4 + b_{05}v^5\right). \end{cases} \tag{4.4}$$

The Hamiltonian function of system $(4.5)|_{\varepsilon=0}$ is

$$H(u,v)=\frac{1}{2}v^2+\frac{1}{2}u^2+\hat{h}_{30}u^3+\hat{h}_{40}u^4,$$

where $\hat{h}_{30}=-\frac{1}{3\hat{\mu}^{\frac{3}{2}}}(1+3ax_c)$ and $\hat{h}_{40}=-\frac{a}{4\hat{\mu}^2}$.

By Theorem 3.1, we get

$$b_{2,0}=2\pi\frac{b_{01}}{\sqrt{\hat{\mu}}},\quad b_{2,1}=\frac{15}{2}\pi\frac{b_{01}}{\sqrt{\hat{\mu}}}\hat{h}_{30}^2+\frac{b_{03}}{\sqrt{\hat{\mu}}}\pi,\quad \dots$$

For the coefficient $c_1(\delta)$ in (4.2) and (4.3), we make a change of variables of the form in system (2.22)

$$\tilde{u}=\sqrt{\tilde{\mu}}(x-x_s),\quad \tilde{v}=y,$$

with a time scaling $t\to\sqrt{\tilde{\mu}}t$, where $\tilde{\mu}=3ax_s^2+2x_s-1>0$.

Then the system (2.22) becomes

$$\begin{cases}\dot{\tilde{u}}=\tilde{v},\\ \dot{\tilde{v}}=\tilde{u}+\frac{1}{\tilde{\mu}^{\frac{3}{2}}}(1+3ax_s)\tilde{u}^2+\frac{a}{\tilde{\mu}^2}\tilde{u}^3\\ \qquad\quad +\frac{1}{\sqrt{\tilde{\mu}}}\varepsilon\left(b_{01}\tilde{v}+b_{02}\tilde{v}^2+b_{03}\tilde{v}^3+b_{04}\tilde{v}^4+b_{05}\tilde{v}^5\right).\end{cases}\tag{4.5}$$

The corresponding Hamiltonian function of system $(4.5)|_{\varepsilon=0}$ is

$$H(\tilde{u},\tilde{v})=\frac{1}{2}\tilde{v}^2-\frac{1}{2}\tilde{u}^2+\tilde{h}_{30}\tilde{u}^3+\tilde{h}_{40}\tilde{u}^4,$$

where $\tilde{h}_{30}=-\frac{1}{3\tilde{\mu}^{\frac{3}{2}}}(1+3ax_s)$ and $\tilde{h}_{40}=-\frac{a}{4\tilde{\mu}^2}$.

Now using the formula in Theorem 3.2, we obtain

$$c_1=-\frac{b_{01}}{\sqrt{\tilde{\mu}}}.$$

To get the coefficients $c_0(\delta)$ and $c_{0i}(\delta)$, $i=1,2$ in (4.2) and (4.3), we apply the formulas in Theorem 3.2 to obtain

$$c_{0i}=\frac{1}{\sqrt{\tilde{\mu}}}\oint_{L_i}\sum_{j=1}^{5}b_{0j}\tilde{v}^j\mathrm{d}\tilde{u}=\frac{1}{\sqrt{\tilde{\mu}}}\sum_{j=1}^{5}b_{0j}I_{ij},\quad c_0=c_{01}+c_{02},$$

where

$$I_{1j}=\oint_{L_1}\tilde{v}^j\mathrm{d}\tilde{u}=\int_{\tilde{u}_-}^{0}[-\tilde{u}f(\tilde{u})]^j\,\mathrm{d}\tilde{u},\quad j=1,\dots,5,$$

$$I_{2j}=\oint_{L_2}\tilde{v}^j\mathrm{d}\tilde{u}=\int_{0}^{\tilde{u}_+}[\tilde{u}f(\tilde{u})]^j\,\mathrm{d}\tilde{u},\quad j=1,\dots,5,$$

where $\tilde{u}_-$ is the intersection point between homoclinic loop L_1 and $\tilde{u}$-axis, $\tilde{u}_+$ is the intersection point between homoclinic loop L_2 and $\tilde{u}$-axis, and $f(\tilde{u})=\sqrt{1-2\tilde{h}_{30}\tilde{u}-2\tilde{h}_{40}\tilde{u}^2}$.

4.2. Number of limit cycles of system (2.22)

So far, we have obtained all coefficients in (4.1), (4.2) and (4.3). Now we use these coefficients to study limit cycles. For convenience, we calculate I_{1j} and I_{2j}, $j = 1, \ldots, 5$ at the beginning, to get

$$
\begin{aligned}
&I_{11} = -0.7474078353, \quad I_{12} = 0.4502699162, \quad I_{13} = -0.2907177904,\\
&I_{14} = 0.1946760298, \quad I_{15} = -0.1333327103;\\
&I_{21} = 0.6598971507, \quad I_{22} = 0.3693171740, \quad I_{23} = 0.2213951892,\\
&I_{24} = 0.1376207262, \quad I_{25} = 0.08748549333.
\end{aligned}
$$

By comparison of the expression of $b_{1,0}$ and $b_{2,0}$, we find that the root of $b_{1,0} = 0$ and the root of $b_{2,0} = 0$ are same, then we solve $b_{1,0} = 0$, we have

$$U = \frac{4s\xi\sqrt{a_1}}{\rho D s_1(r_{y_1} + 2\theta_0 r_{y_2} + 3\theta_0^2 r_{y_3})},$$

substituting the parameter values in Table 1 into which, we obtain $\bar{U} = 3.787861482$.

Then taking $U = \bar{U} = 3.787861482$ to check the value of other coefficients, we get

$$
\begin{aligned}
&b_{1,1} = -3.770583020 \neq 0, \quad b_{2,1} = -3.877758647 \neq 0,\\
&c_{01} = 1.517974242 \neq 0, \quad c_{02} = -0.0379772686 \neq 0, \quad c_0 = 1.479996972 \neq 0.
\end{aligned}
$$

Now we will check if there exists limit cycles between homoclinic loop L_1 and center $(0, 0)$, between homoclinic loop L_2 and center $(x_c, 0)$, and surrounding double homoclinic loop L. Taking $U = \bar{U} = 3.787861482$ and some ε_1, ε_2, ε_3, ε_4, ε_5 positive and sufficiently small, and $h_1 = h_{c_1} + \varepsilon_1$, $h_2 = h_{c_2} + \varepsilon_2$, $h_3 = h_s - \varepsilon_3$, $h_4 = h_s - \varepsilon_4$, $h_5 = h_s + \varepsilon_5$ and $h_6 = h_s + 100$ we have

$$
\begin{aligned}
&M_1(h_1, \bar{U}) = b_{1,1}(\bar{U})\varepsilon_1^2 < 0, \quad M_2(h_2, \bar{U}) = b_{2,1}(\bar{U})\varepsilon_2^2 < 0,\\
&M_1(h_3, \bar{U}) = c_{01}(\bar{U}) > 0, \quad M_2(h_4, \bar{U}) = c_{02}(\bar{U}) < 0,\\
&M(h_5, \bar{U}) = c_0(\bar{U}) > 0, \quad M(h_6, \bar{U}) = c_0(\bar{U}) < 0,
\end{aligned}
$$

which gives

$$
\begin{aligned}
&sgn(M_1(h_1, \bar{U}), M_1(h_3, \bar{U})) = -1, \quad sgn(M_2(h_2, \bar{U}), M_2(h_4, \bar{U})) = 1,\\
&\text{and} \quad sgn(M(h_5, \bar{U}), M(h_6, \bar{U})) = -1.
\end{aligned}
$$

Applying the method in [3], we obtain that there exist 1 limit cycle between homoclinic loop L_1 and center $(0, 0)$, and one limit cycle surrounding the double homoclinic loop L.

Since $b_{2,0} = b_{1,0} = 0$, similar as [3], taking $b_{1,0}$ or $b_{2,0}$ as a free parameter, we can know that there exists one more limit cycle near center $(0, 0)$ or $(x_c, 0)$. Hence, we have following theorem.

Theorem 4.1. *There exists some U near $\bar{U} = 3.787861482$ such that the system (2.22) has at least 3 limit cycles: 1 limit cycle is near one of the center, 1 limit cycle is between homoclinic loop L_1 and center $(0,0)$, and last limit cycle surrounds the double homoclinic loop L.*

Now solving the equation $c_{01} = 0$ yields $\tilde{U}_1 = 19.56011461$, substituting which into coefficients $b_{1,0}$, $b_{2,0}$, c_1, c_{02} and c_0 gets

$$b_{1,0} = 2.693373094 \neq 0, \quad b_{2,0} = 2.769929939 \neq 0,$$
$$c_1 = -0.6152098552 \neq 0, \quad c_{02} = 0.4320541001 \neq 0, \quad c_0 = 0.4320541001 \neq 0,$$

which means there exists one limit cycle near the homoclinic loop L_1. To examine the limit cycle between homoclinic loop L_1 and center $(0,0)$, between homoclinic loop L_2 and center $(x_c, 0)$, and surrounding double homoclinic loop L, taking $U = \tilde{U}_1 = 19.56011461$ and some ε_1, ε_2, ε_3, ε_4, ε_5 positive and sufficiently small, and $h_1 = h_{c_1} + \varepsilon_1$, $h_2 = h_{c_2} + \varepsilon_2$, $h_3 = h_s - \varepsilon_3$, $h_4 = h_s - \varepsilon_4$, $h_5 = h_s + \varepsilon_5$ and $h_6 = h_s + 100$, we have

$$M_1(h_1, \tilde{U}_1) = b_{1,0}(\tilde{U}_1)\varepsilon_1 > 0, \quad M_2(h_2, \tilde{U}_1) = b_{2,0}(\tilde{U}_1)\varepsilon_2 > 0,$$
$$M_1(h_3, \tilde{U}_1) > 0, \quad M_2(h_4, \tilde{U}_1) = c_{02}(\tilde{U}_1) > 0,$$
$$M(h_5, \tilde{U}_1) = c_0(\tilde{U}_1) > 0, \quad M(h_6, \tilde{U}_1) = c_0(\tilde{U}_1) < 0,$$

which shows

$$sgn(M_1(h_1, \tilde{U}_1), M_1(h_3, \tilde{U}_1)) = 1, \quad sgn(M_2(h_2, \tilde{U}_1), M_2(h_4, \tilde{U}_1)) = 1,$$
$$\text{and} \quad sgn(M(h_5, \tilde{U}_1), M(h_6, \tilde{U}_1)) = -1.$$

Similar as [3], we have following theorem.

Theorem 4.2. *There exists some U near $\tilde{U}_1 = 19.56011461$ such that the system (2.22) has at least 2 limit cycles: 1 limit cycle is near homoclinic loop L_1, and 1 limit cycle surrounds the double homoclinic loop L.*

Then, we solve equation $c_{02} = 0$ to have $\tilde{U}_2 = 4.08330378$, and we take $U = \tilde{U}_2 = 4.08330378$ to get

$$b_{1,0} = 0.0504516584 \neq 0, \quad b_{2,0} = 0.0518857038 \neq 0,$$
$$c_1 = -0.0115239724 \neq 0, \quad c_{01} = 1.327461364 \neq 0, \quad c_0 = 1.327461370 \neq 0,$$

and take some ε_1, ε_2, ε_3, ε_4, ε_5 positive and sufficiently small, and $h_1 = h_{c_1} + \varepsilon_1$, $h_2 = h_{c_2} + \varepsilon_2$, $h_3 = h_s - \varepsilon_3$, $h_4 = h_s - \varepsilon_4$, $h_5 = h_s + \varepsilon_5$ and $h_6 = h_s + 100$ we have

$$M_1(h_1, \tilde{U}_2) = b_{1,0}(\tilde{U}_2)\varepsilon_1 > 0, \quad M_2(h_2, \tilde{U}_2) = b_{2,0}(\tilde{U}_2)\varepsilon_2 > 0,$$
$$M_1(h_3, \tilde{U}_2) = c_{01}(\tilde{U}_2) < 0, \quad M_2(h_4, \tilde{U}_2) > 0,$$
$$M(h_5, \tilde{U}_2) = c_0(\tilde{U}_2) > 0, \quad M(h_6, \tilde{U}_2) = c_0(\tilde{U}_2) < 0,$$

which gives

$$sgn(M_1(h_1, \tilde{U}_2), M_1(h_3, \tilde{U}_2)) = -1, \quad sgn(M_2(h_2, \tilde{U}_2), M_2(h_4, \tilde{U}_2)) = 1,$$

and $\quad sgn(M(h_5, \tilde{U}_2), M(h_6, \tilde{U}_2)) = -1.$

Employing the method in [3], we have following theorem.

Theorem 4.3. *There exists some U near $\tilde{U}_2 = 4.08330378$ such that the system (2.22) has at least 3 limit cycles: 1 limit cycle is near homoclinic loop L_2, 1 limit cycle is between homoclinic loop L_1 and center $(0,0)$, and 1 limit cycle surrounds the double homoclinic loop L.*

At last, solving the equation $c_0 = 0$, we obtain $\tilde{U}_3 = 181.8652959$, taking which gets

$$b_{1,0} = 30.40966733 \neq 0, \quad b_{2,0} = 31.27403632 \neq 0,$$
$$c_1 = -6.946058485 \neq 0, \quad c_{01} = -3.380036697 \neq 0, \quad c_{02} = 3.380036697 \neq 0,$$

taking $U = \tilde{U}_3 = 181.8652959$ and some ε_1, ε_2, ε_3, ε_4, ε_5 positive and sufficiently small, and $h_1 = h_{c_1} + \varepsilon_1$, $h_2 = h_{c_2} + \varepsilon_2$, $h_3 = h_s - \varepsilon_3$, $h_4 = h_s - \varepsilon_4$, $h_5 = h_s + \varepsilon_5$ and $h_6 = h_s + 100$ we have

$$M_1(h_1, \tilde{U}_3) = b_{1,0}(\tilde{U}_3)\varepsilon_1 > 0, \quad M_2(h_2, \tilde{U}_3) = b_{2,0}(\tilde{U}_3)\varepsilon_2 > 0,$$
$$M_1(h_3, \tilde{U}_3) = c_{01}(\tilde{U}_3) < 0, \quad M_2(h_4, \tilde{U}_3) = c_{02}(\tilde{U}_3) > 0,$$
$$M(h_5, \tilde{U}_3) = c_1(\tilde{U}_3) < 0, \quad M(h_6, \tilde{U}_3) = c_0(\tilde{U}_3) < 0,$$

which gives

$$sgn(M_1(h_1, \tilde{U}_2), M_1(h_3, \tilde{U}_2)) = -1, \quad sgn(M_2(h_2, \tilde{U}_2), M_2(h_4, \tilde{U}_2)) = 1,$$
$$\text{and} \quad sgn(M(h_5, \tilde{U}_2), M(h_6, \tilde{U}_2)) = 1.$$

Applying the method in [3], we have following theorem.

Theorem 4.4. *There exists some U near $\tilde{U}_3 = 181.8652959$ such that the system (2.22) has at least 2 limit cycles: 1 limit cycle near double homoclinic loop L, and the limit cycle locates between homoclinic loop L_1 and center $(0,0)$.*

5. Numerical simulation

In this section, we present some numerical examples and simulations to demonstrate the theoretical results obtain in previous section, with physical parameter values taken from Table 1. As we mentioned in Section 2, we only consider the low wind velocity $U \leq 20\text{m/s}$.

Taking $U = 3.9$ and the initial value $x(0) = 0.08$, $y(0) = 0$, we give the time evolution of x and the phase portrait of system (2.22) in Figure 4. Figure 4 shows that there indeed exists a limit cycle near center $(0,0)$, and we can demonstrate the limit cycle is stable based on the time evolution and phase portrait. The amplitude of limit cycle is approximately 0.06, timed by dimensionless scale μ_1 in (2.19), which is equal to about 0.22 m in reality.

When we select $U = 3.9$ and the initial value at $x(0) = 2.95$, $y(0) = 0$, the simulation of system (2.22) is shown in Figure 5. It shows a good agreement with

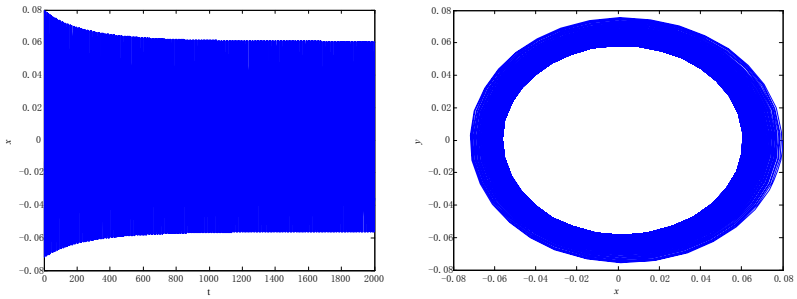

(a) (b)

Figure 4. Simulation of system (2.22) for $U = 3.9$, with initial value $x(0) = 0.08$, $y(0) = 0$, converging to a stable limit cycle: (a) time evolution; and (b) phase portrait.

theoretical prediction, confirming that there is one limit cycle near center $(x_c, 0)$, similarly, from the time evolution and phase portrait, we can determine that it is stable. The amplitude of limit cycle is also approximately 0.06, multiplied by dimensionless scale μ_1 in (2.19), which is equal to about 0.22 m.

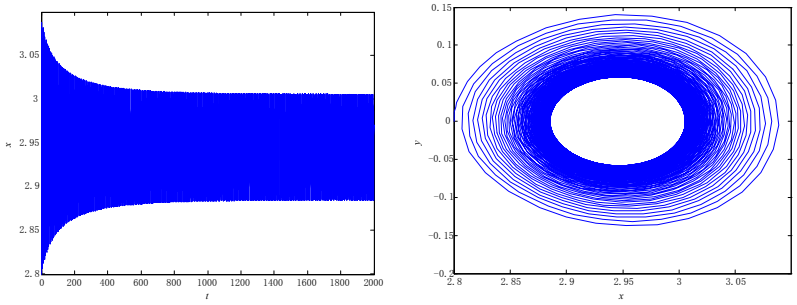

(a) (b)

Figure 5. Simulation of system (2.22) for $U = 3.9$, with initial value $x(0) = 2.95$, $y(0) = 0$, converging to a stable limit cycle: (a) time evolution; and (b) phase portrait.

Further, we conduct a numerical simulation on original system (2.17). When $U = 3.9$, the steady-state time history is shown in Figure 6, from which we can see that the galloping amplitude is nearly 0.22 m. It is in agreement with the theoretical prediction.

At last, taking $U = 19.55$ and initial value $x(0) = -0.62$, $y(0) = 0$, the simulation of system (2.22) is shown in Figure 7. The simulation results indicates the limit cycle near the double homoclinic loop L is unstable, and it will converge to a stable limit cycle surrounding L. The maximal amplitude of limit cycle is about 2.5, which is about 9.17 m in reality. From the steady-state time history of system (2.17) as shown in Figure 8, we can get that the vibration amplitude is about 10 m. The authors conjecture that the reason of the difference between the theoretical and numerical result is induced by high wind velocity.

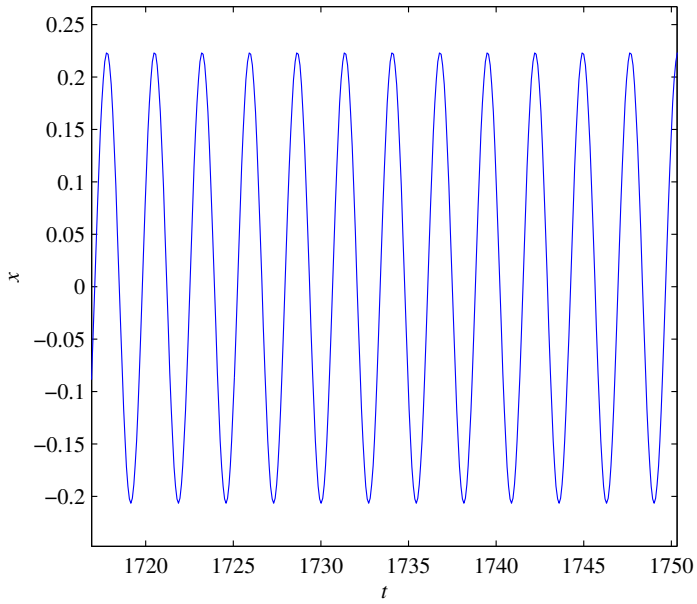

Figure 6. Steady-state time history of system (2.17) for $U = 3.9$.

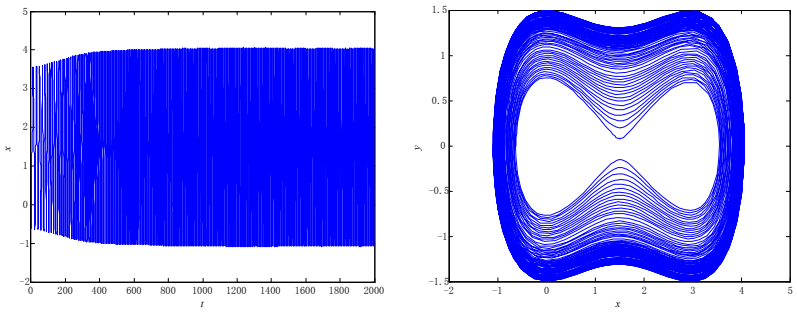

(a) (b)

Figure 7. Simulation of system (2.22) for $U = 19.55$, with initial value $x(0) = -0.62$, $y(0) = 0$, converging to a stable limit cycle: (a) time evolution; and (b) phase portrait.

6. Conclusion and discussion

The in-plane galloping of iced transmission line is researched in this paper. Considering the geometrical and aerodynamical nonlinearities, we get an one-degree-of-freedom model. After rescaling, we get a near-Hamiltonian system, on which we use Melnikov function expansions to study the limit cycles. We find that when the wind velocity is near $U = 3.787861482$, there are at least 3 limit cycles in this model, 1 limit cycle is near one of the center, 1 limit cycle is between homoclinic loop L_1 and center $(0, 0)$, and last limit cycle surrounds the double homoclinic loop L. By employing numerical simulation, we illustrate the theoretical results and determine

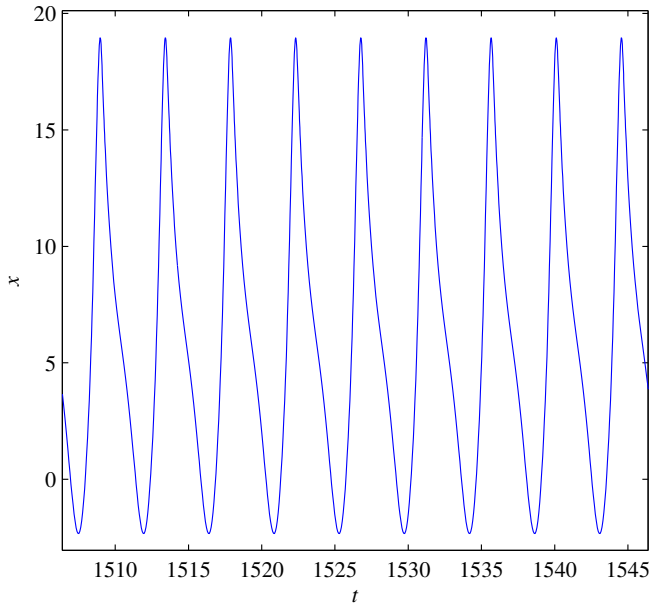

Figure 8. Steady-state time history of system (2.17) for $U = 19.55$.

the stability of these limit cycles.

The results obtained in this paper show that under some engineering and environmental condition, the iced transmission line system may behave stable limit cycle motion, which is harm to the safety of transmission system. Since the motivation of galloping study is to find the mechanism and to make some suggestions on anti-galloping, in future work, we may select other physical parameters as bifurcation parameters to study the limit cycles and to get the optimal physical parameter combinations for avoiding galloping.

The main contribution of this paper is applying Han's method to mechanics, especially to determine the oscillation of in-plane galloping of iced transmission line. The method we used in this paper is also applied to many other disciplines, such as global bifurcations for a generalized codimension-4 Duffing-van der pol equation [12], periodic waves in a population model with density-dependent migrations and Allee Effect [20], and so on.

Acknowledgements

The authors gratefully acknowledge the support of the National Natural Science Foundation of China (51808389), the Project of Shanxi Youth Foundation (201901D211067), the Project of Tianjin Youth Foundation (18JCQNJC08000), and the Scientific and Technological Innovation Programs of Higher Education Institutions in Shanxi (2019L0254). The authors would like to thank Professor Junmin Yang of Hebei Normal University for her valuable suggestions, which greatly improve the presentation of this paper.

Appendix

$$
\begin{aligned}
a_1 &= \frac{\pi^2}{sl^2}\int_0^l \left[\frac{1}{16}EA\left(16y_{0x}^2+9y_{0x}^4\right)-\frac{1}{2}T_0\left(3y_{0x}^2-2\right)\right]\sin^2(\frac{\pi x}{l})\mathrm{d}x,\\
a_2 &= \frac{\pi^3}{sl^3}\int_0^l \left[3T_0-\frac{3}{16}EAy_{0x}\left(16-40y_{0x}^2-y_{0x}^4\right)\right]\sin^2(\frac{\pi x}{l})\cos(\frac{\pi x}{l})\mathrm{d}x,\\
a_3 &= \frac{\pi^4}{sl^4}\int_0^l \frac{3}{4}EA(15y_{0x}^2-2)\sin^2(\frac{\pi x}{l})\cos^2(\frac{\pi x}{l})\mathrm{d}x,\\
b_1 &= \frac{\rho UDs_1}{2s}\left(r_{y_1}+2\theta_0 r_{y_2}+3\theta_0^2 r_{y_3}\right),\\
b_2 &= \frac{\rho Ds_1}{2s}\left[r_{y_1}\theta_0+(1+\theta_0^2)r_{y_2}+(3\theta_0+\theta_0^3)r_{y_3}\right],\\
b_3 &= -\frac{\rho Ds_1}{2sU}\left[r_{y_1}+2\theta_0 r_{y_2}+(1+3\theta_0^2)r_{y_3}\right],\\
b_4 &= \frac{\rho Ds_1}{2sU^2}\left(r_{y_2}+3\theta_0 r_{y_3}\right),\\
b_5 &= -\frac{\rho Ds_1}{2sU^3}r_{y_3},
\end{aligned}
$$

where

$$
\begin{aligned}
s &= \int_0^l m\sin^2(\frac{\pi x}{l})\left(1+\frac{1}{2}y_{0x}^2-\frac{1}{8}y_{0x}^4\right)\mathrm{d}x,\\
s_1 &= \int_0^l \sin(\frac{\pi x}{l})\left(1+\frac{1}{2}y_{0x}^2-\frac{1}{8}y_{0x}^4\right)\mathrm{d}x,
\end{aligned}
$$

References

[1] V. I. Arnold, *Geometrical methods in the theory of ordinary differential equations*, 250, Springer Science & Business Media, New York, 2012.

[2] J. Den Hartog, *Transmission line vibration due to sleet*, Transactions of the American Institute of Electrical Engineers, 1932, 4(51), 1074–1076.

[3] M. Han, H. Yan, J. Yang and C. Lhotka, *On the number of limit cycles of some liénard systems*, Canadian Applied Mathematics Quarterly, 2009, 17(1), 61–83.

[4] M. Han and P. Yu, *Normal forms, Melnikov functions and bifurcations of limit cycles*, 181, Springer Science & Business Media, London, 2012.

[5] D. Hilbert, *Mathematical problems*, Bulletin of the American Mathematical Society, 1902, 8, 437–479.

[6] L. Hou and Y. Chen, *Study on chaos in galloping of the transmission line*, Journal of Vibration Engineering, 2014, 27(1), 75–83.

[7] Y. Hou and M. Han, *Melnikov functions for planar near-hamiltonian systems and hopf bifurcations*, Journal of Shanghai Normal University(Natural Science), 2006, 35(1), 1–10.

[8] B. Liu, K. Zhu, X. Li and X. Zhan, *Hysteresis phenomenon in the galloping of the d-shape iced conductor*, Mathematical Problems in Engineering, 2013, 784239.

[9] B. Liu, K. Zhu, X. Sun et al., *A contrast on conductor galloping amplitude calculated by three mathematical models with different dofs*, Shock and Vibration, 2014, 2014, 781304.

[10] F. Liu, Q. Zhang and Y. Tan, *Analysis of high codimensional bifurcation and chaos for the quad bundle conductor's galloping*, Chinese Physics Letters, 2010, 27(4), 044702.

[11] X. Liu and B. Huo, *Nonlinear vibration and multimodal interaction analysis of transmission line with thin ice accretions*, International Journal of Applied Mechanics, 2015, 7(01), 1550007.

[12] Y. Liu and Y. Chen, *Global bifurcations for a generalized codimension-4 duffing-van der pol equation*, Journal of Vibration and Shock, 2011, 30(1), 69–72.

[13] A. Luongo, D. Zulli and G. Piccardo, *A linear curved-beam model for the analysis of galloping in suspended cables*, Journal of Mechanics of Materials and Structures, 2007, 2(4), 675–694.

[14] A. Luongo, D. Zulli and G. Piccardo, *Analytical and numerical approaches to nonlinear galloping of internally resonant suspended cables*, Journal of Sound and Vibration, 2008, 315(3), 375–393.

[15] P. McComber and A. Paradis, *A cable galloping model for thin ice accretions*, Atmospheric Research, 1998, 46(1), 13–25.

[16] S. Meng and W. Kong, *Design of Overhead Transmission Line*, China Electric Power Press, Beijing, 2007.

[17] O. Nigol and P. Buchan, *Conductor galloping part i-den hartog mechanism*, IEEE transactions on power apparatus and systems, 1981, 2(PAS-100), 699–707.

[18] O. Nigol and P. Buchan, *Conductor galloping-part ii torsional mechanism*, IEEE Transactions on Power Apparatus and Systems, 1981, 2(PAS-100), 708–720.

[19] Z. Qin, Y. Chen, X. Zhan et al., *Research on the galloping and anti-galloping of the transmission line*, International Journal of Bifurcation and Chaos, 2012, 22(02), 1250038.

[20] X. Sun, P. Yu and Q. Bin, *Global existence and uniqueness of periodic waves in a population model with density-dependent migrations and allee effect*, International Journal of Bifurcation and Chaos, 2017, 27(12), 1750192.

[21] Z. Yan, Z. Yan, Z. Li and T. Tan, *Nonlinear galloping of internally resonant iced transmission lines considering eccentricity*, Journal of Sound and Vibration, 2012, 331(15), 3599–3616.

[22] P. Yu, A. Shah and N. Popplewell, *Inertially coupled galloping of iced conductors*, Journal of applied mechanics, 1992, 59(1), 140–145.

[23] Q. Zhang, N. Popplewell and A. Shah, *Galloping of bundle conductor*, Journal of Sound and Vibration, 2000, 234(1), 115–134.